Scientific Research Publishing

Journal of Geoscience and Environment Protection, 2023, 11, 131-160
https://www.scirp.org/journal/gep
ISSN Online: 2327-4344
ISSN Print: 2327-4336

# Towards a Link between Climate Extremes and Thermodynamic Patterns in the City of Rio de Janeiro-Brazil: Climatological Aspects and Identified Changes

**Wanderson Luiz-Silva*, Fabricio Polifke da Silva, Claudine Pereira Dereczynski, José Ricardo de Almeida França**

Department of Meteorology, Institute of Geosciences, Federal University of Rio de Janeiro, Rio de Janeiro, Brazil
Email: *wanderson@igeo.ufrj.br

**How to cite this paper:** Luiz-Silva, W., da Silva, F. P., Dereczynski, C. P., & de Almeida França, J. R. (2023). Towards a Link between Climate Extremes and Thermodynamic Patterns in the City of Rio de Janeiro-Brazil: Climatological Aspects and Identified Changes. *Journal of Geoscience and Environment Protection, 11,* 131-160.
https://doi.org/10.4236/gep.2023.118008

**Received:** July 21, 2023
**Accepted:** August 25, 2023
**Published:** August 28, 2023



## Abstract

Modification signs in extreme weather events may be directly related to alterations in the thermodynamic panorama of the atmosphere that need to be better understood. This study aimed to make a first interconnection between climate extremes and thermodynamic patterns in the city of Rio de Janeiro. Maximum and minimum air temperature and precipitation extreme indices from two surface meteorological stations (ABOV and STCZ) and instability indices based on temperature and humidity from radiosonde observations (SBGL) were employed to investigate changes in the periods 1964-1980 (P1), 1981-2000 (P2), and 2001-2020 (P3). Statistical tests were adopted to determine the significance and magnitude of trends. The frequency of warm (cold) days and warm (cold) nights are increasing (decreasing) in the city. Cold (Warm) extremes are changing with greater magnitude in ABOV (STCZ) than in STCZ (ABOV). In ABOV, there is a significant increase of +84 mm/decade in the rainfall volume associated with severe precipitation (above the 95$^{th}$ percentile) and most extreme precipitation indices show an increase in frequency and intensity. In STCZ, there is a decrease in extreme precipitation until the 1990s, and from there, an increase, showing a wetter climate in the most recent years. It is also verified in SBGL that there is a statistically significant increase (decrease) in air temperature of +0.1˚C/decade (−0.2˚C/decade) and relative humidity of +1.2%/decade (−3%/decade) at the low and middle (high) troposphere. There is a visible rising trend in most of the evaluated instability indices over the last few decades. The increasing trends of some extreme precipitation indices are probably allied to the precipitable water increasing trend of +1.2 mm/decade.

**Keywords**

Climate Change, Climatology, Instability Indices, Precipitation Extremes, Temperature Extremes

## 1. Introduction

Global warming is expected to lead to a significant increase in atmospheric water vapor content and changes in the hydrological cycle, including an intensification of extreme precipitation episodes (O'Gorman & Schneider 2009; Westra et al., 2014). According to the Sixth Assessment Report, AR6 of the Intergovernmental Panel on Climate Change (IPCC 2021), there is evidence that anthropogenic actions have been influencing climate extremes in all regions of the globe, such as heatwaves, severe rainfall, prolonged droughts, and tropical cyclones. On a global scale, extreme precipitation events are projected to intensify by about 7% for every 1˚C of global warming, according to the Clausius-Clapeyron (CC) relationship (Pall et al., 2007).

The precipitation frequency and intensity in a given area can be a function of the interaction between atmospheric phenomena and physiographic aspects of the region, such as ocean and terrain features (Kunz, 2007; Poujol et al., 2020). Besides, the presence of atmospheric ingredients necessary for the generation of extreme convective rainfall is also relevant. Thus, the identification of atmospheric thermodynamic patterns favorable to extreme rainfall, mainly related to convection, such as the availability of moisture at low atmospheric levels (Emanuel, 1994; Doswell III, 2001) and instability indices (or convective parameters) are fundamental (Rasmussen & Blanchard, 1998; DeRubertis, 2006).

Particularly during the warmest period of the year (summer), the presence of specific meteorological systems creates favorable atmospheric conditions for heavy precipitation (Boers et al., 2015). Concerning short-term forecasting, severe local storms in Brazil are sometimes related to high rainfall rates, which are still a daily challenge for operational routine and the scientific community seeking to improve numerical forecasting methods (Lopez, 2007; Schumacher & Peters, 2017). Thus, given these circumstances in the atmosphere, instability indices have been a valuable tool for diagnosing and predicting intense precipitation (Doswell III & Schultz, 2006).

A climatology of the atmosphere's thermodynamic characteristics can help understand the large-scale physical processes that lead to precipitation formation (Brooks et al., 2007). The climatological distribution of instability indices may not be helpful for forecasting weather, but it may aid in understanding the probability of a given event in different locations (Taszarek et al., 2018). Furthermore, possible changes over the years in the thermodynamic parameters, mainly those related to air temperature and humidity, can be analyzed and associated with global climate change.

Since precipitable water in the atmosphere has a crucial effect on the energy balance, it is also important to evaluate its behavior. Based on reanalysis data, Paltridge et al. (2009) show that specific and relative humidity have been increasing at low levels in the troposphere and decreasing at high levels over the Southern Hemisphere since the mid-twentieth century. Zveryaev and Chu (2003) had already confirmed that the tropospheric water vapor content over the tropical portion of Brazil has been growing considerably since the 1970s. In this sense, through observational data *in loco*, some recent studies have shown an elevation in the frequency and intensity of extreme weather and climate events associated with air temperature and precipitation in Brazil over the last decades, for instance, in the scale of watersheds (Zandonadi et al., 2016; Luiz-Silva et al., 2019), in the coast (Zilli et al., 2017), in the Amazon (Marengo et al., 2018), in the Northeast (Costa et al., 2020), and in the whole Brazil (Dereczynski et al., 2020; Regoto et al., 2021).

In the Southeastern region of Brazil, the most intense precipitation is recorded in the austral summer due to enhanced heat and moisture supply, often associated with dynamic forcings generated by frontal systems and the South Atlantic Convergence Zone, SACZ (Carvalho et al., 2004; Luiz-Silva et al., 2021). In the State of Rio de Janeiro, Zilli et al. (2017) and Luiz-Silva and Oscar-Júnior (2022) show that the frequency of rainy days is decreasing, but with a significant elevation in the precipitation intensity related to extreme events, which in turn may be related to thermodynamic effects, such as an increase in the convective instability. In the city of Rio de Janeiro, the second largest in Brazil, there is expressive interaction between weather systems and physiographic aspects such as topography, vegetation, proximity to the ocean, and the presence of two large bays. This mechanism, associated with the vulnerability of the urban perimeter, is the main triggering factor for disasters such as floods and landslides in the face of heavy precipitation (Nunes et al., 2020). Silva et al. (2019a; 2020) state that the vertical coupling of moisture flow convergence at low atmospheric levels and mass flow divergence at higher levels is one of the leading dynamic triggers for intense rainfall in Rio de Janeiro. In the long term, Dereczynski et al. (2013) and Luiz-Silva and Dereczynski (2014) confirm the growth in accumulated precipitation related to severe rainfall since the late twentieth century in the city.

Given the evident modification in the thermodynamics of the planet due to climate change (Shepherd, 2014), the main objective of this work is to examine preliminarily the thermodynamic behavior of the atmosphere associated with climate extremes over the city of Rio de Janeiro, considering historical averages and detected trends. Thus, climate extremes associated with observed air temperature and precipitation *in situ* are revisited, and temperature and humidity patterns in altitude are investigated. In addition, the instability indices *K*, Total Totals (*TT*), and Precipitable Water (*PW*) are analyzed concerning the climatology and observed trends, considering the registered precipitation intensity. Therefore, we seek a better elucidation of thermodynamic mechanisms asso-

ciated with verified trends in air temperature and rainfall in the city of Rio de Janeiro over the last years.

## 2. Methodology

### 2.1. Study Area

The city of Rio de Janeiro, capital of the State of Rio de Janeiro, is located in the Southeastern region of Brazil (Figure 1) and presents an area of about 1200 km$^2$ with an estimated population of around 6.8 million inhabitants (IBGE, 2021). According to Alvares et al. (2014), the city of Rio de Janeiro shows a predominantly tropical climate: high temperatures and accumulated precipitation concentrated especially during the austral spring and summer, and a cooler and drier climate throughout the austral autumn and winter. The average maximum (minimum) temperature in the city of Rio de Janeiro in the summer is 32.0˚C (23.0˚C), and in the winter, it is 26.0˚C (17.0˚C). The average rainfall in summer (total from December to February) is 450 mm, while in winter (total from June

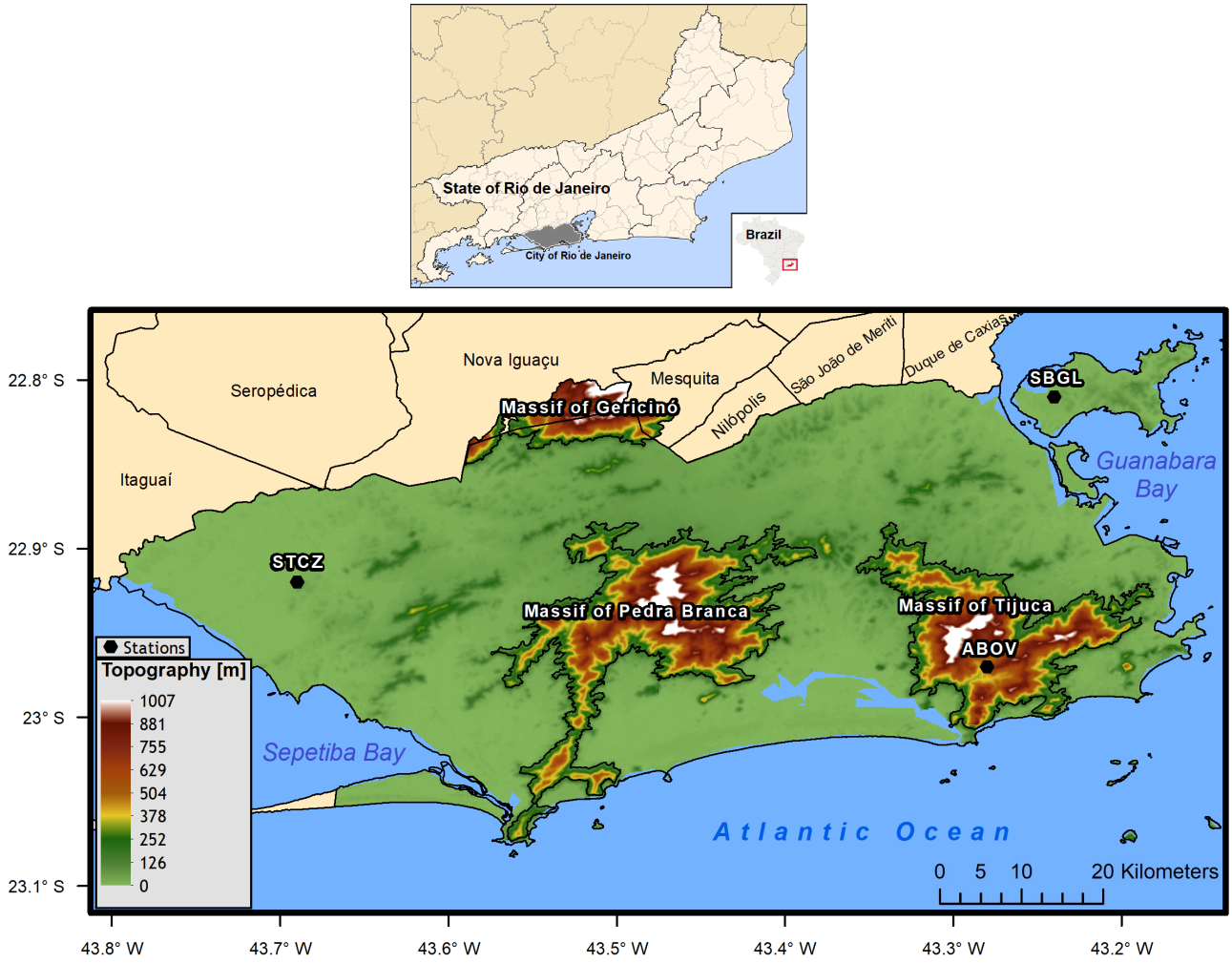


Figure 1. City of Rio de Janeiro and location of INMET meteorological stations (Alto da Boa Vista, ABOV and Santa Cruz, STCZ) and FAB upper-air station (SBGL) at Galeão International Airport.

to August), it is 150 mm (Luiz-Silva & Dereczynski, 2014). In terms of topography, the city has three massifs (Tijuca, Pedra Branca, and Gericinó). The climate is also influenced by two bays (Guanabara and Sepetiba), the Atlantic Ocean, in addition to the presence of islands, sandbanks, lagoons, and rivers. Originally, the vegetation was exuberant and mainly composed of the Atlantic Forest. However, the forest suppression and irregular occupation have significantly increased the city's vulnerabilities to flooding, landslides, and the urban heat islands (La Rovere & Silva de Sousa, 2016). These risks are exacerbated by climate change, with intense exposure for residents of precarious settlements that are especially threatened (Barata et al., 2020).

### 2.2. Data

Daily air maximum and minimum temperature and precipitation data come from two available meteorological stations of the Brazilian National Institute of Meteorology (INMET) located in different points of Rio de Janeiro: Alto da Boa Vista (ABOV), located in a forested area and with lower urban density in its surroundings, at an altitude of 341 m; and Santa Cruz (STCZ), located in the western city at an altitude of 63 m, in a less vegetated region, and with a larger urban densification (**Figure 1**). Both stations are located in the metropolitan region of Rio de Janeiro, which has an accentuated population density and urban perimeter around it. These weather stations are conventional and the only ones with good quality and quantity of data in the city of Rio de Janeiro, and without changes in their locations. Data are available in the INMET meteorological database (BDMEP, https://bdmep.inmet.gov.br/). In ABOV, the data comprise the period 1967-2020, while in STCZ, the datasets cover the period 1964-2018. The ABOV and STCZ climatology data were analyzed into three 20-year periods: P1 (1964-1980); P2 (1981-2000); and P3 (2001-2020). So, it is possible to assess how much historical averages have changed in the city of Rio de Janeiro over these past periods. Regoto et al. (2021), for instance, show more significant warming in the 1980s and 1990s in Brazil.

The ABOV and STCZ data series have a few shortcomings. However, the absence of information in some specific years does not affect the conclusion about identified trends in both stations. ABOV has flaws (few months without data) from 6 years: 1990, 1991, 2008, 2009, 2016 and 2017. STCZ has no observed data between 1995 and 1997.

This work uses radiosonde data (1973-2020) launched by the Brazilian Air Force (FAB) at the Galeão International Airport (SBGL), Rio de Janeiro, at 12 UTC (09:00 local time). These data, available at the Wyoming University website (http://weather.uwyo.edu/upperair/sounding.html) are used to investigate the vertical profile of temperature and relative humidity, and instability indices (described in Section 2.3.2). Reports from standard pressure level were employed to produce the mean tropospheric profiles.

The distance between SBGL and ABOV is 17.4 km, and between SBGL and

STCZ is 47.5 km. The SBGL station is considered representative of the city of Rio de Janeiro as it is located only about 17 km from the nearest surface station used in this study (ABOV). For instance, considering atmospheric phenomena of the meso-beta scale (20 - 200 km), meteorological systems and their effects can be well captured.

## 2.3. Atmospheric Indices

### Climate Extremes Indices

According to Easterling et al. (2000), society and nature are thoroughly affected by any alteration in the frequency and intensity of climate extremes episodes. Some climate extreme indicators are based on daily data of precipitation (PRCP), maximum temperature (TX), and minimum temperature (TN) (Frich et al., 2002). In this research, 25 indices were selected (**Table 1**) for the analysis of climatology and trends in the city of Rio de Janeiro. The RClimDex software (Zhang et al., 2018) was employed to calculate these indicators.

Physical conditions expressed by thermodynamic and dynamic indices can characterize the atmospheric potential for intense/extreme precipitation formation. These parameters are commonly called instability indices. Each index, or ingredient, presents its strengths and weaknesses. So, no single index can provide a complete characterization of the state of the atmosphere (Kunz, 2007). Therefore, it would be inappropriate to expect that any single index works optimally in all locations or that any index can achieve the best performance for all types of convective storms (Blanchard, 1998). **Table 2** shows the atmospheric parameters evaluated in this work.

The $K$ index is calculated by the sum of the dry bulb ($T_{850}$) and the dew point ($Td_{850}$) temperatures at 850 hPa, subtracted from the dew point depression at 700 hPa (dry bulb $T_{700}$ and dew point $Td_{700}$) and the dry bulb temperature ($T_{500}$) at 500 hPa (George, 1960). It tends to capture conditions favorable to storm formation better when moisture is present throughout the troposphere, as it is a typical feature of tropical environments (DeRubertis, 2006). $K$ values above 30˚C indicate a high potential for the occurrence of storms with heavy rainfall, while $K$ values above 40˚C point to an extremely high possibility of an extreme storm event (Nascimento, 2005).

The Total Totals ($TT$) index is similar to the $K$ index, with the main difference that it does not consider the dew point depression at 700 hPa (Miller, 1972). If an air mass is warm and moist, $K$ and $TT$ indices suggest similar interpretations. However, when an air mass is cooler and drier, $TT$ will produce better results by assigning greater weight to the presence of cold air at medium levels (Silva Dias, 1987). In general, $TT$ values above 40˚C indicate favorable situations for the formation of storms, and values above 50˚C indicate atmospheric conditions for the occurrence of severe weather (Henry, 2000; Nascimento, 2005).

The precipitable water content ($PW$) represents a vertical integration ($dp$) of the water vapor mixing ratio ($w$) between 1000 and 100 hPa. It expresses the

**Table 1.** Climate extremes indices analyzed in this study based on maximum temperature (TX), minimum temperature (TN), and precipitation (PRCP).

| Indices | Definition |
|---|---|
| | **Maximum Temperature** |
| TMAXmean | Mean maximum temperature [˚C] |
| SU30 | Annual count of days when TX ≥ 30˚C [days] |
| TX10p | Percentage of days when TX < 10$^{th}$ percentile [%days] |
| TX90p | Percentage of days when TX > 90$^{th}$ percentile [%days] |
| TXn | Annual minimum value of daily TX [˚C] |
| TXx | Annual maximum value of daily TX [˚C] |
| WSDI | Warm spell duration index – Annual count of days with at least 6 consecutive days when TX > 90$^{th}$ percentile [days] |
| | **Minimum Temperature** |
| TMINmean | Mean minimum temperature [˚C] |
| TR20 | Annual count of days when TN ≥ 20˚C [days] |
| TN10p | Percentage of days when TN < 10$^{th}$ percentile [%days] |
| TN90p | Percentage of days when TN > 90$^{th}$ percentile [%days] |
| TNn | Annual minimum value of daily TN [˚C] |
| TNx | Annual maximum value of daily TN [˚C] |
| CSDI | Cold spell duration index – Annual count of days with at least 6 consecutive days when TN < 10$^{th}$ percentile [days] |
| DTR | Daily temperature range [˚C] |
| | **Precipitation** |
| PRCPTOT | Annual total precipitation [mm] |
| R10mm | Annual count of days when PRCP ≥ 10 mm [days] |
| R30mm | Annual count of days when PRCP ≥ 30 mm [days] |
| R95p | Annual total PRCP when daily PRCP > 95$^{th}$ percentile [mm] |
| R99p | Annual total PRCP when daily PRCP > 99$^{th}$ percentile [mm] |
| RX1day | Annual maximum 1-day precipitation [mm] |
| RX5day | Annual maximum consecutive 5-day precipitation [mm] |
| SDII | Simple precipitation intensity index – PRCPTOT/wet days [mm·day$^{-1}$] |
| CDD | Consecutive dry days – Maximum number of consecutive days with PRCP < 1 mm [days] |
| CWD | Consecutive wet days – Maximum number of consecutive days with PRCP > 1 mm [days] |

**Table 2.** Instability and moisture parameters evaluated in this research.

| Variable | Formula |
|---|---|
| $K$ index | $K = (T_{850} + Td_{850}) - (T_{700} - Td_{700}) - T_{500}$ |
| Total Totals ($TT$) | $TT = (T_{850} + Td_{850}) - 2 * T_{500}$ |

**Continued**

| | |
|---|---|
| Precipitable Water ($PW$) | $PW = \frac{1}{\rho g}\int_{1000}^{100} w dp$ |
| Convective Available Potential Energy (CAPE) | $g\int_{\mathrm{LFC}}^{\mathrm{LNB}} \frac{T_{vp}(z) - T_v(z)}{T_v(z)} \mathrm{d}z$ |

amount of water obtained if the vapor in a unitary horizontal cross-section atmosphere column is condensed and precipitated, where ρ is the air density, and $g$ is the gravity.

The Convective Available Potential Energy index (CAPE) is the vertical integration (d$z$) of the variation between the virtual temperature of the parcel ($Tvp$) and the virtual temperature of the neighboring ambiance ($Tv$) at distinct levels onward the track through which the parcel ascends voluntarily, from the level of free convection (LFC) to the level of neutral buoyancy (LNB), where $g$ is the gravity. The LNB usually indicates the top of convective clouds or the level of divergence. Therefore, this index expresses the energy that a parcel will have when lifted (in J/kg), as well as the potential strength of updrafts in a storm (Derubertis, 2006). When the CAPE index is greater than zero (typically above 1000 J/kg), the atmosphere has the potential for convection, and severe thunderstorms can be expected. Thus, the higher the CAPE value, the more prone the atmosphere is to deep convection formation in the presence of dynamic forcing (Nascimento, 2005; Silva et al., 2019b).

## 2.4. Statistical Tests

The Mann-Kendall non-parametric test (Mann, 1945; Kendall & Stuart, 1975; Sneyers, 1990) is used to assess the statistical significance of trends in climate extremes and instability indices. The null hypothesis considered is the non-existence of growing or declining trends in the time series. Besides, this technique assumes that the sequence of values occurs independently, and that the probability distribution remains stable, that is, the data does not need to belong to a specific distribution. The confidence level adopted is 95%, which corresponds to a significance level α of 5%.

The Sen's Curvature test (Sen, 1968) is used to analyze the magnitude of the trends. It is also a non-parametric method that assumes a linear trend in the data series. The test is calculated as follows:

$$\mathrm{SEN} = \mathrm{median}\left(\frac{x_j - x_i}{j - i}\right), \forall j > i, \tag{1}$$

where $x_j$ is the value of the variable in a specific period (for example, a year) and $x_i$ is the value of the variable in the previous period.

Sen's Curvature test is insensible to outliers and absent information, thus being more realistic and accurate than a simple linear regression. Mann-Kendall and Sen's Curvature tests are very efficient for determining trends in climatological and hydrological series when compared to other parametric methods

(Helsel & Hirsch 1992).

## 3. Results and Discussion

### 3.1. Temperature Extremes

First, it is important to highlight the differences in temperature values between ABOV and STCZ. ABOV is located in a higher altitude and is surrounded by the Atlantic Forest (dense forest biome on the eastern coast of Brazil), while STCZ is near the sea level, in a region where significant urbanization has taken place. Figure 2 highlights the climatological differences between some climate extremes indices associated with air temperature in ABOV and STCZ. Figure 2(a) (Figure 2(b)) shows the distribution of TMAXmean (TMINmean) between 1964 and 2020 and highlights the high frequency (more than 90% of data) of annual mean maximum (minimum) temperatures between 25˚C and 27˚C (17˚C and 19˚C) in ABOV and 28˚C to 30˚C (19˚C to 21˚C) in STCZ. When verifying the frequency of days with a maximum temperature above 30˚C (SU30, Figure 2(c)) and the frequency of nights with a minimum temperature above 20˚C (TR20, Figure 2(d)), the difference is also discrepant between these two areas of the city. There is a higher frequency of about 50 to 100 days in ABOV and around 150 to 200 days in STCZ for both SU30 and TR20, so STCZ has more warm days and nights compared to ABOV.

The climatology and trends of the climate extremes indices associated with temperature (Table 1) in ABOV and STCZ is shown in Table 3. In general, the temperature extremes indices show warming in the city, with the most considerable changes occurring between P1 and P2, mainly for the warm extremes (Table 3), where the magnitude rates of increasing trends are greatest. TMAXmean in ABOV (STCZ) increased from 25.7˚C (28.9˚C) in P1 to 26.9˚C (29.8˚C) during P2 and then remained the same average in P3. TMINmean in ABOV (STCZ) was 17.7˚C (19.9˚C) in P1, and in P3 is 18.3˚C (20.4˚C). The increase in TMAXmean and TMINmean is clearly exhibited by the boxplots in Figure 3(a) and Figure 3(b).

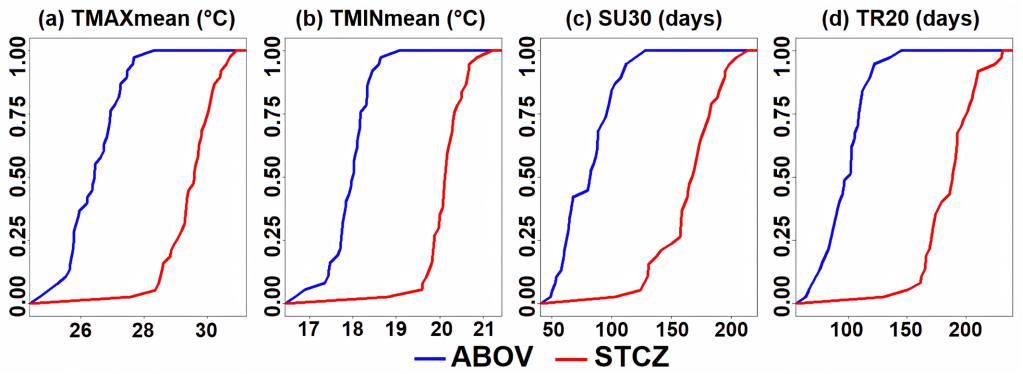


Figure 2. Cumulative distribution function (CDF) diagrams of the indices associated with air temperature (a) TMAXmean, mean maximum temperature (˚C), (b) TMINmean, mean minimum temperature (˚C), (c) SU30, annual count of days when TX ≥ 30˚C (days), and (d) TR20, annual count of days when TN ≥ 20˚C (days) in ABOV (blue line) and STCZ (red line) in the period 1964-2020.

Table 3. P1, P2, and P3 climatologies and detected trends (Sen's curvature for total period) in climate extremes of air temperature in ABOV and STCZ. Boldfaced values of trends were considered statistically significant at the 95% confidence level by the Mann-Kendall test.

| Index (Annual Mean) | ABOV | | | STCZ | | | Observed Trend (per decade) | |
|---|---|---|---|---|---|---|---|---|
| | P1: 1964-1980 | P2: 1981-2000 | P3: 2001-2020 | P1: 1964-1980 | P2: 1981-2000 | P3: 2001-2020 | ABOV | STCZ |
| **Maximum Temperature** | | | | | | | | |
| TMAXmean (˚C) | 25.7 ± 0.5 | 26.9 ± 0.6 | 26.9 ± 0.7 | 28.9 ± 0.8 | 29.8 ± 0.6 | 29.8 ± 0.7 | **+0.3** | **+0.3** |
| SU30 (days) | 64 ± 12 | 86 ± 19 | 92 ± 20 | 143 ± 25 | 174 ± 16 | 177 ± 21 | **+7.5** | **+9.6** |
| TX10p (%days) | 13.5 ± 4.1 | 6.6 ± 2.7 | 8.1 ± 2.6 | 13.2 ± 5.0 | 7.9 ± 3.2 | 10.8 ± 3.4 | **−1.2** | **−0.6** |
| TX90p (%days) | 7.7 ± 2.3 | 12.3 ± 5.3 | 13.2 ± 4.2 | 8.6 ± 3.4 | 11.7 ± 4.8 | 14.6 ± 4.2 | **+1.3** | **+1.8** |
| TXn (˚C) | 15.6 ± 0.9 | 16.2 ± 1.3 | 16.0 ± 1.3 | 17.8 ± 1.3 | 17.6 ± 0.9 | 17.5 ± 1.1 | +0.1 | 0.0 |
| TXx (˚C) | 36.2 ± 1.0 | 36.2 ± 1.3 | 37.0 ± 1.2 | 39.3 ± 1.1 | 39.4 ± 1.2 | 40.5 ± 1.3 | **+0.3** | **+0.3** |
| WSDI (days) | 1 ± 2 | 6 ± 6 | 4 ± 7 | 1 ± 3 | 2 ± 3 | 4 ± 6 | 0.0 | 0.0 |
| **Minimum Temperature** | | | | | | | | |
| TMINmean (˚C) | 17.7 ± 0.4 | 17.8 ± 0.6 | 18.3 ± 0.4 | 19.9 ± 0.4 | 20.1 ± 0.3 | 20.4 ± 0.4 | **+0.1** | **+0.1** |
| TR20 (days) | 86 ± 12 | 88 ± 31 | 110 ± 17 | 173 ± 20 | 187 ± 15 | 197 ± 20 | **+5.5** | **+6.2** |
| TN10p (%days) | 11.8 ± 6.0 | 10.3 ± 4.9 | 7.5 ± 3.9 | 11.1 ± 6.4 | 8.8 ± 1.6 | 7.7 ± 3.5 | **−0.7** | **−0.6** |
| TN90p (%days) | 8.6 ± 3.8 | 9.5 ± 5.2 | 14.5 ± 5.4 | 8.4 ± 3.4 | 12.0 ± 3.2 | 15.0 ± 4.8 | **+1.5** | **+1.8** |
| TNn (˚C) | 10.5 ± 0.9 | 9.8 ± 1.5 | 10.5 ± 1.2 | 12.2 ± 1.3 | 11.8 ± 1.2 | 12.8 ± 1.1 | 0.0 | +0.1 |
| TNx (˚C) | 25.0 ± 1.0 | 25.3 ± 1.8 | 24.8 ± 0.8 | 26.4 ± 0.8 | 26.5 ± 0.6 | 27.2 ± 0.9 | −0.1 | **+0.3** |
| CSDI (days) | 4 ± 8 | 6 ± 14 | 2 ± 3 | 4 ± 7 | 1 ± 3 | 2 ± 4 | 0.0 | 0.0 |
| **Daily Temperature Range** | | | | | | | | |
| DTR (˚C) | 8.0 ± 0.4 | 9.1 ± 0.6 | 8.7 ± 0.5 | 9.0 ± 0.5 | 9.7 ± 0.4 | 9.4 ± 0.4 | **+0.2** | **+0.1** |

Warm (cold) days and nights are becoming more (less) frequent in the city of Rio de Janeiro (Table 3). TX90p in ABOV increased from 7.7% warm days a year in P1 to 12.3% warm days a year in P2, then showed a lower increase during P3, reaching 13.2% warm days a year. The increase in TN90p was a little more pronounced, going from 8.6% (8.4%) in P1 to 14.5% (15.0%) in P3 in ABOV (STCZ), as also evidently illustrated in Figure 3(c). Regarding cold extremes, for example, TX10p in ABOV (STCZ) reduced from 13.5% (13.2%) cold days a year in P1 to 6.6% (7.9%) cold days a year in P2 and finally increased to 8.1% (10.8%) cold days a year in P3. Comparing ABOV and STCZ trends magnitudes, it is clear that cold (warm) extremes are changing with greater magnitude in ABOV (STCZ) than in STCZ (ABOV). Especially in STCZ, the frequency of TXx above 40˚C has increased considerably in P3 (Figure 3(d)). The same urbanization process that differentiates temperatures between ABOV and STCZ has contributed to their increases over the last few decades throughout the city of Rio de Janeiro.

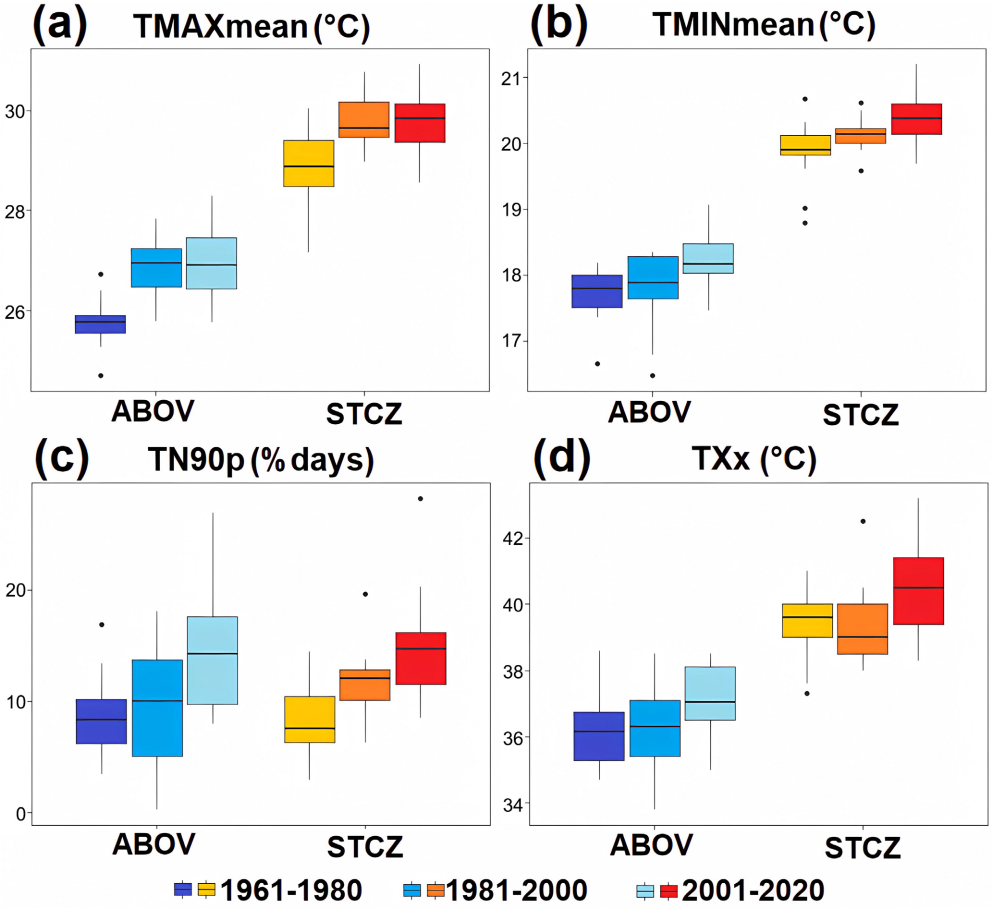


**Figure 3.** Boxplots comparing the evolution of the climate extremes indices related with air temperature (a) TMAXmean, mean maximum temperature (˚C), (b) TMINmean, mean minimum temperature (˚C), (c) TN90p, percentage of days when TN > 90$^{th}$ percentile (%days), and (d) TXx, annual maximum value of daily TX (˚C) in ABOV and STCZ during P1, P2, and P3. In the boxplots, the box denotes the interquartile range, where the base of the box marks the first quartile (Q1) and the top of the box marks the third quartile (Q3). The line inside the box depicts the median. Whiskers symbolize the lower (Q1 − 1.5 * (Q3 − Q1)) and upper (Q3 + 1.5 * (Q3 − Q1)) limits of the distribution. Dots beyond these limits are considered outliers.

Concerning the observed trends in the period 1964-2020, most of them show statistically significant warming (Table 3). Warm extremes are increasing in intensity (TMAXmean, TXx, TNx) and frequency (TX90p, TN90p, SU30, TR20), showing an increased number in warm days and warm nights. Trends for cold extremes are positively associated with their intensity (TMINmean, TNn, TXn) but negatively related with their frequencies (TX10p, TN10p), showing reduction in cold days and cold nights. Most of the detected trends indicate statistically significant warming for both meteorological stations, and the warming rates of TMAXmean are +0.3˚C/decade and TMINmean are +0.1˚C/decade. This stronger rise in maximum temperatures also increases the daily temperature range (DTR) with a magnitude of +0.2˚C/decade in ABOV and +0.1˚C/decade in STCZ (Table 3). The observed trends show an increase of +1.3% (+1.8%) in warm days a year per decade and +1.5% (+1.8%) in warm nights a year per decade in ABOV

(STCZ), and also a decrease of −1.2% (−0.6%) of cold days a year per decade and −0.7% (−0.6%) of cold nights a year per decade in ABOV (STCZ).

When analyzing the anomalies of some warm extremes indices (Figure 4), it is noted that, despite presenting positive trends throughout the studied period, their values went from negative to positive from the 1990s onwards. As of the 2000s, the frequency of warm days (TX90p) is already 10% above the climatology in Rio de Janeiro (Figure 4(a)). The increase in the frequency of warm nights (TN90p) is also quite evident in the distribution of values over the years (Figure 4(b)). It is also verified that the historical averages of the absolute extreme indices have gotten higher; that is, the highest maximum (TXx) and minimum (TNx) temperatures keep rising in the city. TXx increased from an average of 36.2˚C in ABOV in P1 to 37.0˚C in P3, while in STCZ, the values went from 39.3˚C to 40.5˚C (Table 3). Figure 4(c) shows that TXx is already up to +3˚C above the historical average in the 2010s in ABOV and STCZ. TNx showed no trend in ABOV, but in STCZ it grew +0.3˚C/decade (Figure 4(d)). The average duration of heatwaves (WSDI) also increased from 1960s to 2010s (figure not shown).

Specific studies should be conducted to attribute the leading causes of warming to the city of Rio de Janeiro. For instance, Peres et al. (2018) show through land use maps the effect of urbanization on the temperature of Rio de Janeiro,

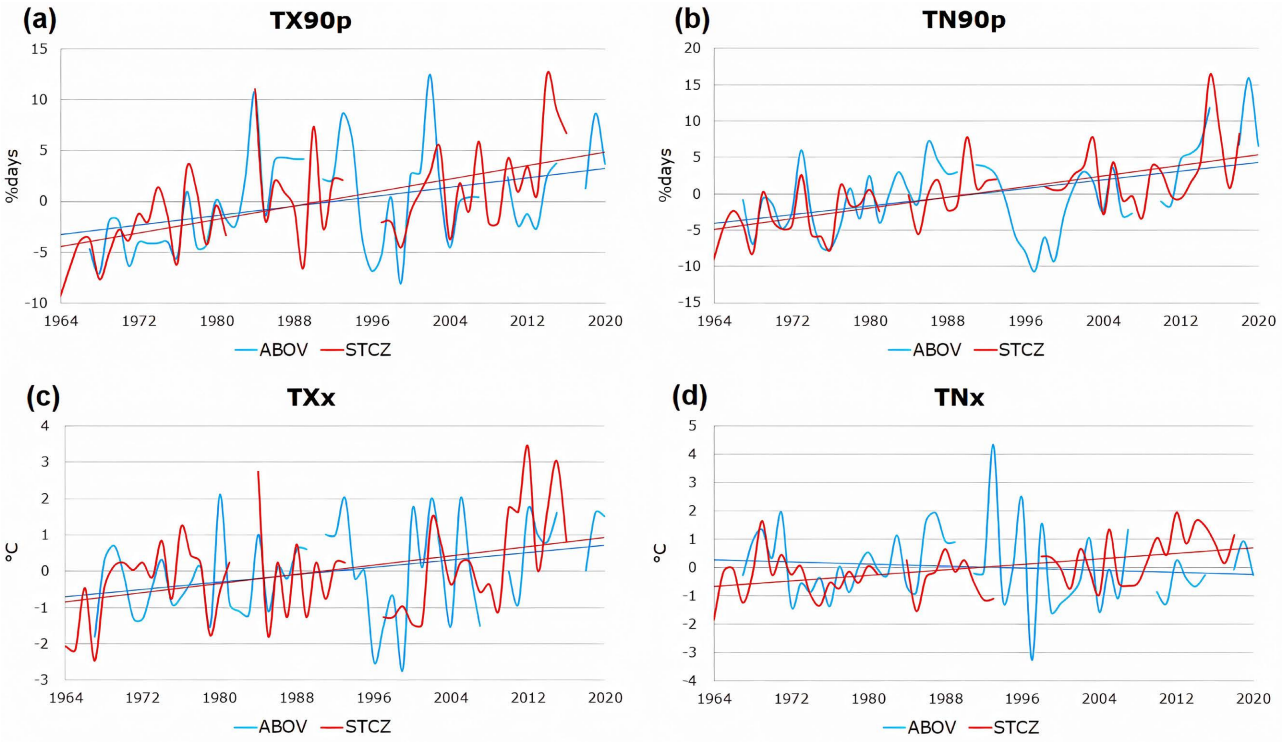


Figure 4. Time series and observed trends of the anomalies of indices associated with air temperature (a) TX90p, percentage of days when TX > 90$^{th}$ percentile (%days), (b) TN90p, percentage of days when TN > 90$^{th}$ percentile (%days), (c) TXx, annual maximum value of daily TX (˚C), and (d) TNx, annual maximum value of daily TN (˚C) in ABOV (blue line) and STCZ (red line) in the period 1964-2020.

including the significant increase during the 2010s compared to the 1990s. Besides, warm days are often recorded under atmospheric blockings during the warmest seasons in the Southeastern Brazil, and such events have become more frequent over the last few years (Geirinhas et al., 2021).

### 3.2. Precipitation Extremes

Once again, the physiographic aspects of Rio de Janeiro (particularly the relief) demarcate considerable differences in the city's climatology, this time in terms of accumulated rainfall (**Figure 5**). The Tijuca massif in association with the evapotranspiration of local vegetation favors high total precipitation in ABOV, especially in the windward of the mountains, which receives the sea breeze (Dereczynski et al., 2013). The relief slopes facilitate the rise of air around ABOV, cloud formation, and rainfall, mainly during the passage of frontal systems. In STCZ, precipitation is also caused by frontal systems and local convection. The distribution of total annual rainfall from 1964 to 2020 shows that variability is somewhat greater in ABOV than in STCZ (**Figure 5(a)**). PRCPTOT values predominate from 500 to 1500 mm in STCZ and between 1500 and 3000 in ABOV. The frequency of R10mm (moderate or heavy precipitation) varies from 20 to 40 days in STCZ and 40 to 60 days in ABOV (**Figure 5(b)**). **Figure 5(c)** shows that R99p of ABOV is nearly double that of STCZ and once again showing greater variability (slightly steeper curve). STCZ presents a slightly higher amount of CDD than ABOV (**Figure 5(d)**), because this last one presents several aspects promoting precipitation more frequently (even of low intensity), such as the relief and proximity to the sea.

The climatology and trends of the climate extremes indices related to precipitation (**Table 1**) in ABOV and STCZ are shown in **Table 4**. When comparing the climatologies of the three 20-year periods climatologies, it is observed that in ABOV most extreme precipitation indices show an increase in frequency and intensity. However, most of them are not considered statistically significant at

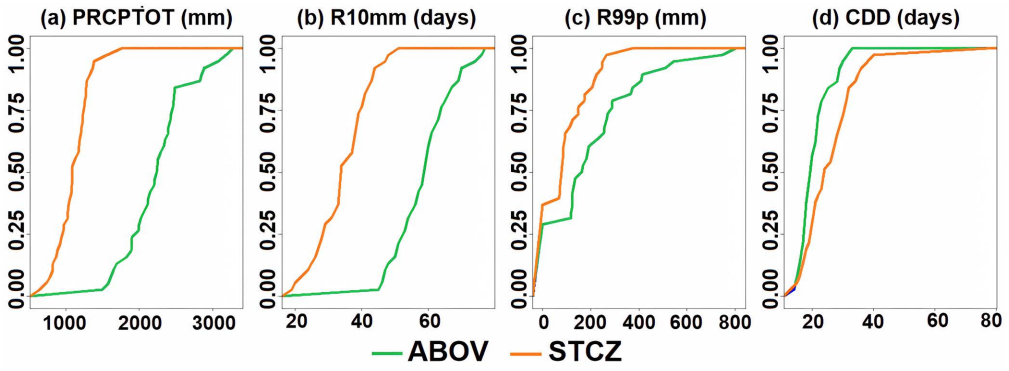


**Figure 5.** Cumulative distribution function (CDF) diagrams of the indices related with precipitation (a) PRCPTOT, annual total precipitation (mm), (b) R10mm, annual count of days when PRCP ≥ 10 mm (days), (c) R99p, annual total PRCP when daily PRCP > 99$^{th}$ percentile (mm), and (d) CDD, maximum number of consecutive days with PRCP < 1 mm (days) in ABOV (green line) and STCZ (orange line) in the period 1964-2020.

Table 4. P1, P2, and P3 climatologies and identified trends (Sen's curvature for total period) in climate extremes of precipitation in ABOV and STCZ. Boldfaced values of trends were considered statistically significant at the 95% confidence level by the Mann-Kendall test.

| Index (Annual Mean) | ABOV | | | STCZ | | | Observed Trend (per decade) | |
|---|---|---|---|---|---|---|---|---|
| | P1: 1964-1980 | P2: 1981-2000 | P3: 2001-2020 | P1: 1964-1980 | P2: 1981-2000 | P3: 2001-2020 | ABOV | STCZ |
| PRCPTOT (mm) | 2207 ± 426 | 2302 ± 529 | 2432 ± 543 | 1190 ± 290 | 885 ± 301 | 1239 ± 227 | +69.0 | +3.6 |
| R10mm (days) | 60 ± 7 | 61 ± 10 | 60 ± 10 | 37 ± 9 | 26 ± 13 | 39 ± 8 | −0.4 | 0.0 |
| R30mm (days) | 23 ± 5 | 23 ± 6 | 24 ± 8 | 8 ± 4 | 5 ± 3 | 10 ± 3 | +0.6 | 0.0 |
| R95p (mm) | 524 ± 350 | 648 ± 348 | 808 ± 371 | 372 ± 216 | 173 ± 151 | 381 ± 147 | **+84.0** | −2.2 |
| R99p (mm) | 196 ± 217 | 185 ± 258 | 333 ± 292 | 135 ± 132 | 48 ± 73 | 130 ± 98 | +13.1 | 0.0 |
| RX1day (mm) | 130 ± 28 | 146 ± 64 | 178 ± 53 | 94 ± 36 | 63 ± 34 | 91 ± 29 | +8.9 | −1.7 |
| RX5day (mm) | 228 ± 71 | 222 ± 88 | 274 ± 68 | 139 ± 57 | 107 ± 53 | 152 ± 43 | **+12.2** | +1.3 |
| SDII (mm/day) | 18.7 ± 2.4 | 18.5 ± 3.3 | 20.6 ± 3.6 | 12.2 ± 2.4 | 9.6 ± 2.8 | 12.6 ± 1.7 | +0.6 | 0.0 |
| CDD (days) | 22 ± 6 | 18 ± 5 | 21 ± 4 | 28 ± 15 | 30 ± 12 | 26 ± 6 | 0.0 | 0.0 |
| CWD (days) | 8 ± 2 | 9 ± 2 | 8 ± 3 | 6 ± 1 | 7 ± 2 | 6 ± 2 | −0.2 | 0.0 |

the 95% confidence level, expect for R95p and RX5day. Despite the increase of +225 mm in PRCPTOT between P1 and P3 in ABOV, this growth is not considered statistically significant. On the other hand, in STCZ the total precipitation (PRCPTOT) and all the extreme precipitation indices decrease from P1 to P2 and then rise from P2 to P3. Considering CDD, its behavior is the opposite, it increases from P1 to P2 and the decreases until P3. All these changes in the climate extreme trend's signal suggest a wetter climate in the recent past (P3).

The precipitation extremes represented by the RX1day and RX5day indices are usually recorded under favorable atmospheric conditions on the regional scale for heavy rainfall (mainly low-level moisture flux convergence centers) in a short period (Silva et al., 2019a) in association with the physiography of the city of Rio de Janeiro. RX1day went from 130 mm to 178 mm in ABOV, comparing the three climatologies examined in this study (Table 4). According to Costa et al. (2018), the city's growth over the last years is marked by several landfills in lakes and coastal portions, changes in the drainage network, and the deforestation of slopes and their occupation, favoring floods and landslides in the face of such extreme precipitation episodes. Also, according to Table 4, RX5day increased from 228 mm (139 mm) in P1 to 274 mm (152 mm) in P3 in ABOV (STCZ). The accumulated rainfall associated with heavy precipitation (R95p and R99p) is higher in the P3 climatology and highlight that ABOV records more intense rainfall episodes than STCZ (Table 4). In ABOV, R95p (R99p) decreased from 524 mm (196 mm) in P1 to 808 mm (333 mm) in P3.

In Figure 6, it is clear that R30mm, RX1day, and SDII increased in ABOV and STCZ from P2 to P3. Figure 6(a) shows that nearly 75% of the years analyzed detected at least 20 days with rainfall above 30 mm. Figure 6(b) highlights

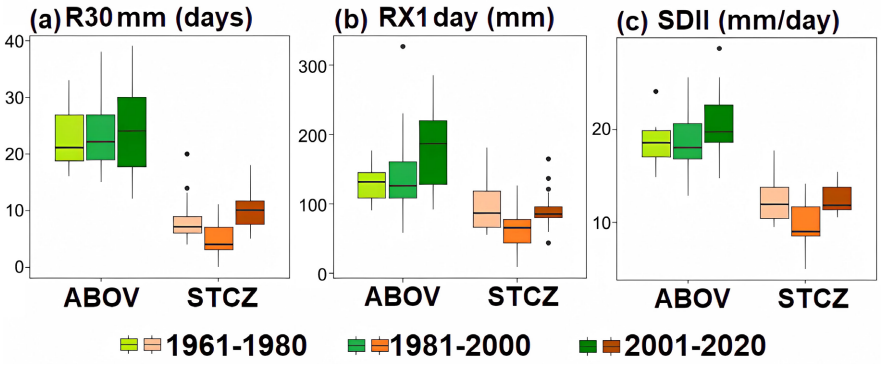


**Figure 6.** Boxplots comparing the evolution of the climate extremes indices associated with precipitation (a) R30mm, annual count of days when PRCP ≥ 30 mm (days), (b) RX1day, annual maximum 1-day precipitation (mm), and (c) SDII, annual total precipitation/wet days (mm/day) in ABOV and STCZ over the last few years: P1, P2, and P3. In the boxplots, the box denotes the interquartile range, where the base of the box marks the first quartile (Q1) and the top of the box marks the third quartile (Q3). The line inside the box depicts the median. Whiskers symbolize the lower (Q1 − 1.5 * (Q3 − Q1)) and upper (Q3 + 1.5 * (Q3 − Q1)) limits of the distribution. Dots beyond these limits are considered outliers.

the increase of RX1day in ABOV mainly from the 2000s onwards. There is also an increase in precipitation intensity (SDII) in the city of Rio de Janeiro, from 18.7 mm/day to 20.6 mm/day in ABOV and from 12.2 mm/day to 12.6 mm/day in STCZ when comparing historical averages for P1 and P3 (**Table 4** and **Figure 6(c)**). The consecutive dry (CDD) and wet (CWD) days did not show any significant trend during the last few years. According to the most recent climatology (P3), CDD lasts about 21 days in ABOV and 26 days in STCZ. In turn, CWD lasts around 8 days in ABOV and 6 days in STCZ (**Table 4**).

**Figure 7** presents the time series of the PRCPTOT, R30mm, R95p, and RX5day anomalies in ABOV and STCZ. First, there is the marked interannual variability of precipitation caused by lower frequency phenomena, such as El Niño-Southern Oscillation (Timmermann et al., 2018) and South Atlantic Dipole (Bombardi et al., 2014), which modulate the frequency and intensity of systems such as fronts and cyclones in the Southeastern region of Brazil. In ABOV, despite the statistically non-significant trends, PRCTOT increased by +69 mm/decade (**Figure 7(a)**) and R30mm increased by +0.6 day/decade (**Figure 7(b)**). The R95p time series highlights the significant increase in severe precipitation in ABOV of +85 mm/decade (**Figure 7(c)**). Dereczynski et al. (2013) had already identified in a shorter dataset in ABOV that R95p was significantly increasing. The RX5day growth was also statistically significant for ABOV (**Figure 7(d)**), with a +12.2 mm/decade rise rate (**Table 4**). In STCZ, there is a decrease in the precipitation (PRCPTOT) and its extremes (R30mm, R95p, RX5day) until the 1990s, and from there, there is an increase in the values, showing a wetter climate in the most recent years.

According to O'Gorman (2015) changes in extreme precipitation are attributed

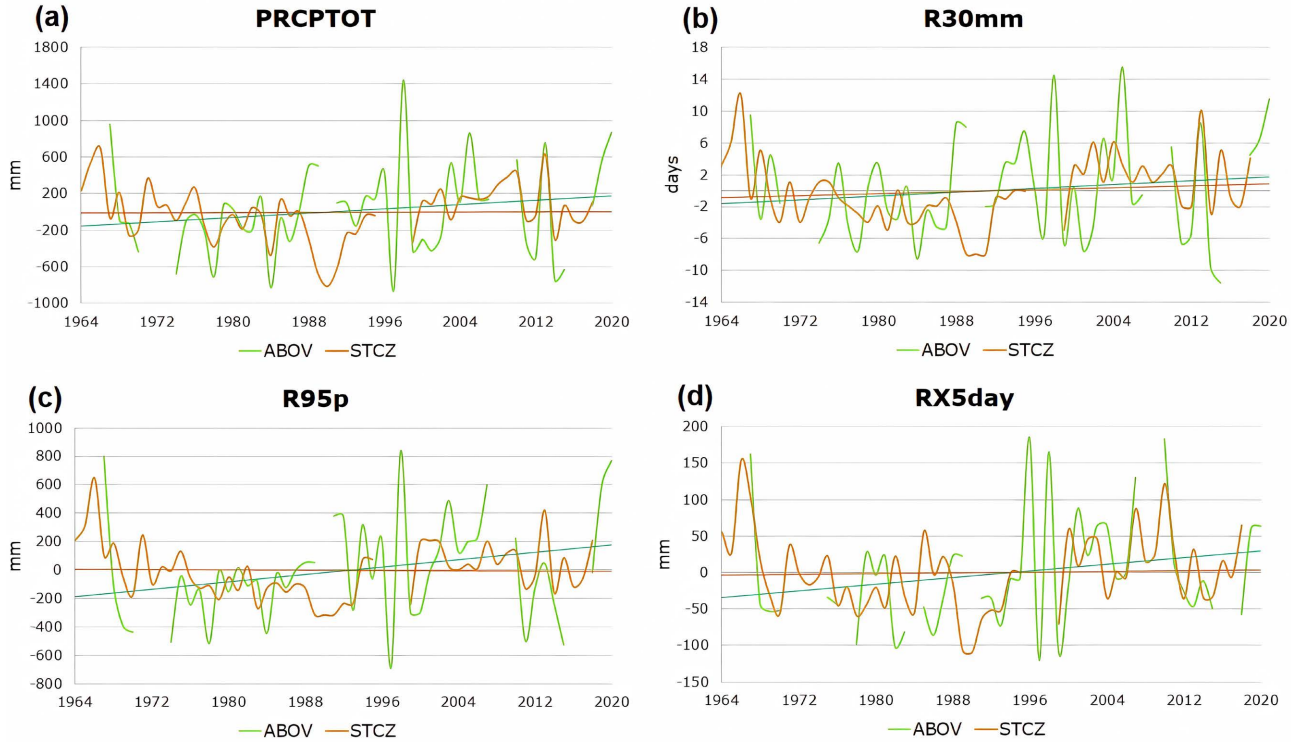


**Figure 7.** Time series and observed trends of the anomalies of indices related with precipitation (a) PRCPTOT, annual total precipitation (mm), (b) R30mm, annual count of days when PRCP ≥ 30 mm (days), (c) R95p, annual total PRCP when daily PRCP > 95$^{th}$ percentile (mm), and (d) RX5day, annual maximum consecutive 5-day precipitation (mm) in ABOV (green line) and STCZ (orange line) in the period 1964-2020.

to the atmospheric thermodynamic and dynamic drivers. As stated early, the thermodynamic process is regulated by the CC Equation, which states that an increase in the global mean air temperature by 1˚C leads to an increase of the atmospheric moisture by 7%, approximately (Trenberth et al., 2003; Held & Soden, 2006; Allan et al., 2020). However, besides the thermodynamic, also various dynamic factors influence the relationship between extreme rainfall and atmospheric temperature (Westra et al., 2013). As seen previously, for Rio de Janeiro we found an increase in precipitation extremes at the ABOV station, being statistically significant for R95p and RX5 day.

Future work may more directly associate the relationship between the frequency and intensity of synoptic-scale meteorological systems with precipitation trends in the city of Rio de Janeiro. For instance, Zilli et al. (2019) show evidence of increasing average daily precipitation along the poleward margin of the climatological SACZ, likely related to a poleward shift of the convergence zone. This is more noticeable over the coastal and oceanic portions of the SACZ, along the Southeastern Brazil.

### 3.3. Climatology and Trends in Upper-Air Observations

The mean tropospheric profiles and the respective trends of air temperature and relative humidity over the period 1973-2020 in SBGL are presented in **Figure 8**.

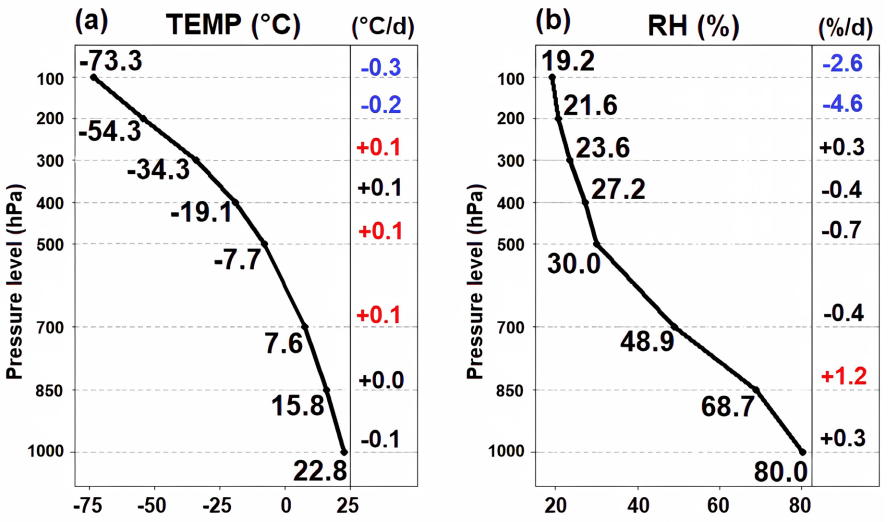


Figure 8. Annual climatology (along the graphs lines) and recorded trends (right side of the graphs) of air temperature, TEMP (˚C) and relative humidity, RH (%) by pressure levels in the atmosphere based on the upper-air observations from SBGL in the period 1973-2020. Red color of the trends means statistically significant increase and blue color represents statistically significant decrease.

As expected, it is noted that temperature and relative humidity decrease with altitude. The climatological data shows temperatures below the freezing point starting in 700 hPa (Figure 8(a)). Relative humidity reduces from 80% to 50% (30% to 20%) from mean sea level to 700 hPa (from 500 to 100 hPa) (Figure 8(b)).

The right side of the graphs in Figure 8 shows the magnitudes of the trends detected over the last few decades in the troposphere around the city of Rio de Janeiro (SBGL). It is verified that there is a statistically significant increase in air temperature at almost all levels in the middle troposphere between 700 hPa and 300 hPa (Figure 8(a)). This fact may be associated with enhanced latent heating relative to more frequent deep moist convection over the region, but it needs deeper investigation. In contrast, the air temperature is decreasing at high levels (200 and 100 hPa). As is known, the air temperature at low and medium levels has been rising due to the increase in the emission of greenhouse gases by anthropogenic forcings (IPCC, 2021), such as carbon dioxide and methane. These gases absorb the infrared radiation emitted by the surface and cause additional atmospheric warming. On the other hand, as greenhouse gases trap more heat in the lower atmosphere, less heat reaches the upper troposphere and stratosphere, causing cooling of this part of the atmosphere (Mears & Wentz, 2009; Randel et al., 2017). Furthermore, other studies indicate that the decrease in ozone in the lower stratosphere at the end of the 20th century also reduced the air temperature in this portion of the atmosphere (Steiner et al., 2020). The trends in the lower levels of the troposphere (such as 1000 hPa), using 12 UTC soundings temperature data, is not so remarkable as if we were using minimum or maximum temperature at 2 meters high, as found by

Gulev et al. (2021).

Concerning atmospheric relative humidity in SBGL, there is a significant increase in the 850 hPa level, against a decrease in 200 and 100 hPa, at the highest levels (**Figure 8(b)**). As the air temperature rises near the surface, there is more evapotranspiration from forest and ocean and moisture offer in the troposphere and, consequently, an increase in relative humidity, as observed at lower levels. Leyba et al. (2019) show an increase of sea surface temperature (SST) in the South Atlantic Ocean and therefore an intensification of heat fluxes, which can contribute to the moistening of the lower troposphere surrounding. It is worth emphasizing the uncertainties inherent to air humidity *in situ* measures in the upper troposphere and stratosphere, regions characterized by a small fraction of the total water vapor in the atmosphere (Miloshevich et al., 2009). Sapucci et al. (2005) evaluated five of the major commercial radiosonde manufacturers. The results show that the humidity measurements achieved by the different sensors were quite similar in the lower atmospheric levels (with a bias median of about 1.8%) and they were quite dispersed in the higher atmospheric layers (root mean square around 14.9%). It could call into question the identified trends here, and these preliminary results should be considered with caution, since we do not know if and how the sensor has changed over the analyzed period. Some works at a global level demonstrate a moistening of the upper troposphere over the last few years and that this cannot be explained solely by natural causes but mainly by atmospheric warming induced by anthropogenic influence (Soden et al., 2005; Chung et al., 2014).

### 3.4. Instability and Moisture Parameters Features

As seen previously, instability indices are traditionally derived from radiosonde profiles. These indices combine measurements of thermal and moisture properties in a vertical profile of the atmosphere. Changes in these thermodynamic patterns are directly associated with modifications in the frequency and intensity of extreme weather events (**Table 3** and **Table 4**), especially those related to precipitation. **Figure 9** shows the anomalies of *K*, *TT*, *PW*, and CAPE (**Table 2**) in SBGL between 1973 and 2020. A clear growing trend is noted in the *K*, *TT*, and *PW* indices, indicating an increasingly unstable atmosphere over the last few years. Perhaps the absolute moistening of the lower troposphere enhances *K* and *TT*. However, there is a decreasing trend in the CAPE index pointing simultaneously to a reduction in the atmospheric environment favorable to convective development. According to the Mann-Kendall statistical test, all these growth trends were considered significant at the 95% confidence level. The magnitude of the *K*, *TT*, *PW*, and CAPE trends were +0.9˚C/decade, +0.2˚C/decade, +1.1 mm/decade, and −40.3 J/kg.decade, respectively.

The increase in air temperature in the midtroposphere and humidity in the lower troposphere (**Figure 8**) contributes to the increase in the *K* index (**Figure 9(a)**), which naturally exhibits higher values in tropical regions, such as

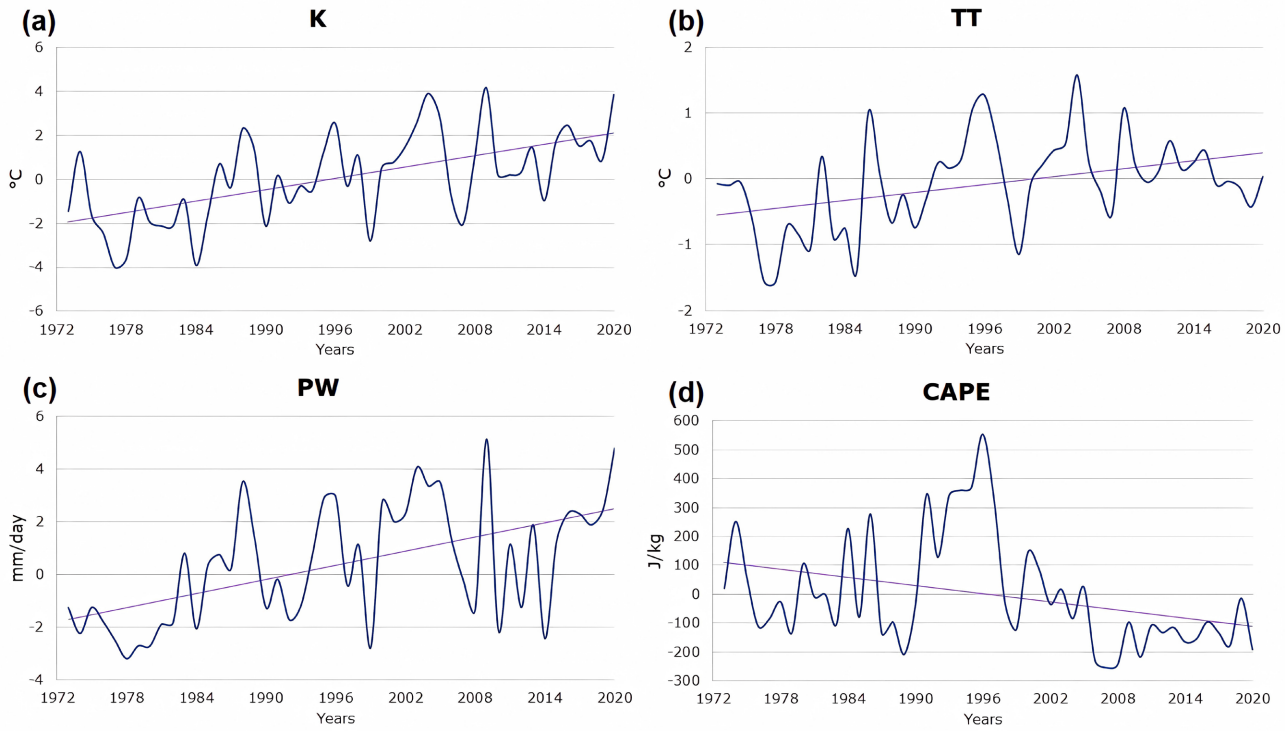


**Figure 9.** Time series of the instability indices anomalies (a) *K* (˚C), (b) *TT* (˚C), (c) *PW* (mm/day), and (d) CAPE (J/kg) measured on the upper-air observations from SBGL in the period 1973-2020.

Rio de Janeiro. In the 1970s, *K* had a mean value of 24.1˚C, and in the 2010s, this average reached 27.4˚C (+1.2˚C above average). The growth of the *TT* index is more modest (**Figure 9(b)**), because it does not incorporate the 700 hPa level in its calculation, which also showed a significant increase in air temperature.

The *PW* increasing trend (**Figure 9(c)**) reflects the addition of water vapor in the troposphere, maybe as a function of the growth in evapotranspiration from the forest and ocean induced by the increase in surface air temperature, concerning the mean and the extremes (**Table 3**). The enhanced moisture convergence by the SACZ (Zilli et al., 2019) or the higher SSTs from the surrounding ocean (Leyba et al., 2019) also could favor this feature, so it needs further investigation. TMAXmean has grown around +1.0˚C over the past five decades in the city. The mean *PW* values increased from about 39.2 mm to 42.3 mm (+8% or +1.1 mm above average). It may have contributed to the increase in PRCPTOT in ABOV (+9%) and STCZ (+15%) over the years, even without statistical significance (**Table 4**). According to Kunkel et al. (2020), *PW* clearly plays a crucial role in the amount of precipitation observed in the upper tail of the precipitation distribution.

Regarding the decreasing trends detected in the CAPE index (**Figure 9(d)**), considering the air parcel theory and its strong dependence on diurnal heating, we believe that the measurements collected and analyzed here do not represent the buoyancy conditions since they correspond to the time of 12 UTC (morn-

ing in Brazil). In general, the highest air temperature variation rates throughout the daytime occur mainly near the surface (Seidel et al., 2005), as in the city of Rio de Janeiro (Silva et al., 2020). Above the 850 hPa level, the air temperature change rates between morning and afternoon are minimal, which do not affect, for example, the results of the *K* and *TT* indices examined early. The most recommendable is to apply the maximum surface temperature method (Doswell III, 2001) for future studies. This method aims to replace the temperature data closest to the surface, collected by a radiosonde launched in the morning, by the temperature values observed in the afternoon, in order to estimate the thermodynamic potential at that time. In this way, the possibly identified trends in the CAPE index could be more realistic concerning the recorded.

The annual climatology of instability indices in the city of Rio de Janeiro concerning some rainfall thresholds is presented in the boxplots in **Figure 10**. Here the instability indices are divided into 3 (three) distinct classes according to the recorded daily precipitation at the ABOV station, the one closest to the upper-air soundings in SBGL: P75 (PRCP ≥ 75$^{th}$ percentile = 20.2 mm/day); P90 (PRCP ≥ 90$^{th}$ percentile = 43.6 mm/day); and P95 (PRCP ≥ 95$^{th}$ percentile = 64.7 mm/day). We seek an initial analysis of the relationship between instability

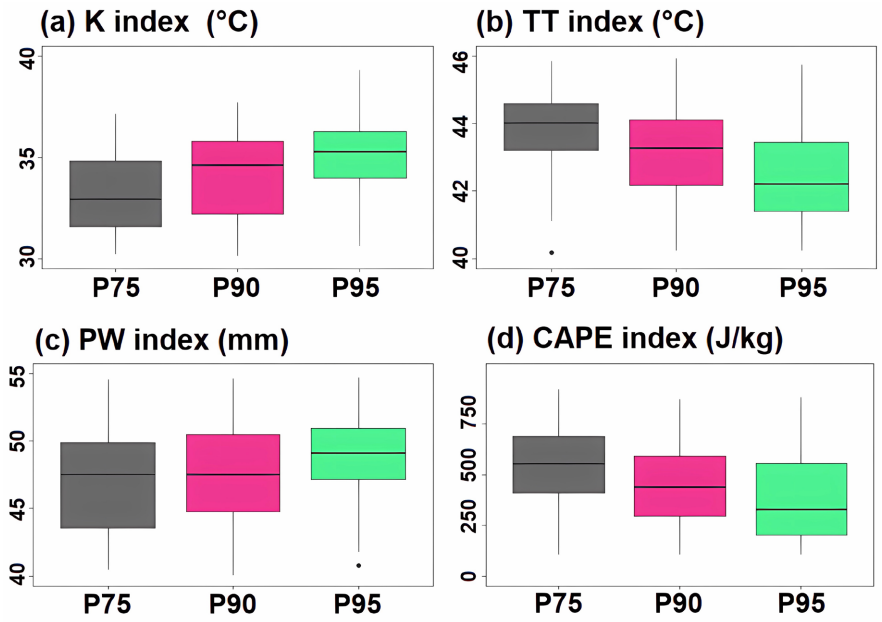


**Figure 10.** Boxplots with the climatology of instability indices (a) *K* (˚C), (b) *TT* (˚C), and (c) *PW* (mm) measured on the upper-air observations from SBGL in the period 1973-2020 according to the 3 (three) classes of precipitation intensity in ABOV: P75 (PRCP ≥ 75$^{th}$ percentile = 20.2 mm/day); P90 (PRCP ≥ 90$^{th}$ percentile = 43.6 mm/day); and P95 (PRCP ≥ 95$^{th}$ percentile = 64.7 mm/day). In the boxplots, the box denotes the interquartile range, where the base of the box marks the first quartile (Q1) and the top of the box marks the third quartile (Q3). The line inside the box depicts the median. Whiskers symbolize the lower (Q1 − 1.5 * (Q3 − Q1)) and upper (Q3 + 1.5 * (Q3 − Q1)) limits of the distribution. Dots beyond these limits are considered outliers.

indices and precipitation intensity, especially the daily precipitation totals that make up the climate extreme indices R95p and R99p. As seen previously, R95p shows a statistically significant increasing trend in ABOV (**Table 4**). In **Figure 10**, it is noted that as the precipitation thresholds grow (P75 to P95), the mean values of the *K* and *PW* indices also increase. On the other hand, there is a reduction in the *TT* and CAPE indices as the precipitation intensity rises.

Commonly, *K* index presents higher values in austral summer, as it is essentially composed of the air temperature, which is higher in this season. *PW* index is also higher in austral summer due to higher air temperatures that cause greater evaporation and moisture supply to the troposphere. It can be seen that the highest values of *K* (about 35˚C) and *PW* (around 49 mm) indices are associated with more severe rainfall, which allows them to be probably related to the values of extreme precipitation indices such as R30mm (**Figure 10(a)** and **Figure 10(c)**). The proximity of the city of Rio de Janeiro to the sea also makes the efficient precipitation production due to a wetter boundary layer and high values of liquid water content (Schumacher & Houze Jr., 2003; Mitovski et al., 2010; Duarte et al., 2018). In austral summer, the thermodynamics of convective movements due to warm air promotes the development of clouds and precipitation showers in the city of Rio de Janeiro (Silva et al., 2019a). In austral winter, a stronger dynamic forcing is needed with sufficient humidity for more expressive rainfall, particularly during the passage of cold fronts or post-frontal rain (Bonnet et al., 2018).

The slightly lower values of the *TT* (about 42˚C) and CAPE (around 300 J/kg) indices for the highest precipitation thresholds suggest that the air temperature at 850 hPa and the parcel's surface temperature would be a little lower in conditions of more accentuated rainfall accumulation (**Figure 10(b)** and **Figure 10(d)**). Probably this can be associated with the type of precipitation that predominates in the austral summer and winter in the city of Rio de Janeiro. During the austral summer, convective storms due to warm and moisture conditions concentrate the greatest rainfall volumes. In contrast, the total precipitation in austral winter and part of the austral autumn and spring is primarily due to stratiform rain with lower air temperatures, as in several areas of Brazil (Tremblay, 2005). Therefore, the expressive amounts of rainfall associated with extreme events can be caused by intermittent precipitation from warm (shallow) clouds for consecutive hours. The highest frequency of daily precipitation above the 95th percentile in ABOV occurred in the austral autumn (March to May).

**Figure 11** shows the trends and magnitudes of instability indices for each precipitation class in ABOV over the period 1973-2020. Note that the *K* and *PW* indices showed statistically significant elevating trends at the 95% confidence level by the Mann-Kendall test for the P75 and P90 classes. The most significant growth trend in *K* index (**Figure 11(a)**) is related to rainfall in P90 (+1.0˚C/decade). Concerning *TT* index (**Figure 11(b)**), there are not significant

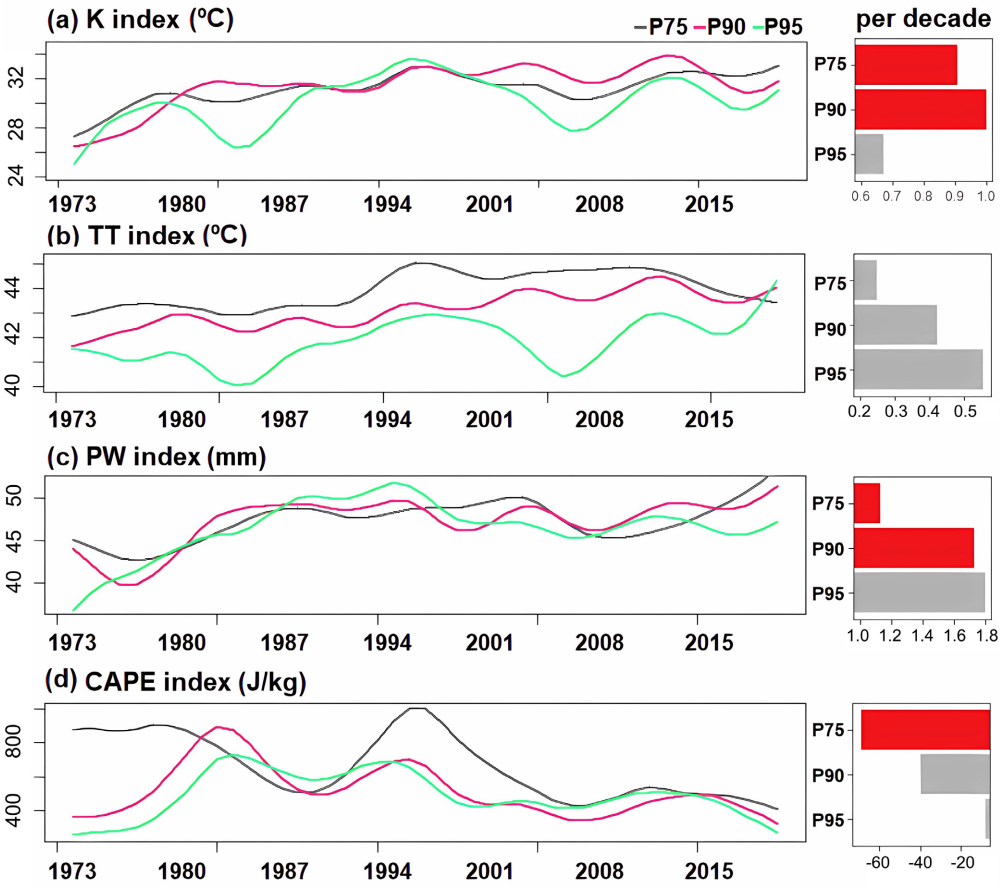


Figure 11. Time series of the annual mean instability indices (a) *K* (˚C), (b) *TT* (˚C), and (c) *PW* (mm) measured on the upper-air observations from SBGL in the period 1973-2020 according to the 3 (three) classes of precipitation intensity in ABOV: P75 (PRCP ≥ 75$^{th}$ percentile = 20.2 mm/day); P90 (PRCP ≥ 90$^{th}$ percentile = 43.6 mm/day); and P95 (PRCP ≥ 95$^{th}$ percentile = 64.7 mm/day). The right side of the figure shows the magnitude of trends (per decade). Red bars denote statistically significant trends at the 95% confidence level.

trends. Regarding the *PW* index (Figure 11(c)), the most significant trend is also associated with P90 (+1.7 mm/decade). It indicates that the atmospheric thermodynamic conditions for heavy precipitation have become considerably even more favorable for severity over the past few decades. However, significant decreasing trends were found to CAPE index (Figure 11(d)) concerning P75 (−68.8 J/kg.decade).

These results possibly explain the increasing trends of almost all extreme climate temperature indices in the city of Rio de Janeiro, besides precipitation indices R95p and RX5day in ABOV (Table 3 and Table 4). As previously mentioned, studies demonstrate that the observed extreme rainfall rises with the air temperature approximately by the CC rate. So, the elevation in air temperature can be related to the growth in precipitation water, increasing the frequency and intensity of extreme rainfall events. However, some researches indicate that atmospheric water vapor content may rise at a higher rate than that mentioned by CC (Fujita & Sato, 2017).

## 4. Conclusion and Final Remarks

This research aimed to make an initial relationship between climate extremes and the environmental conditions of the atmosphere in the city of Rio de Janeiro over the last few decades. It is essential to understand the evolution of the extreme precipitation characteristics associated with thermodynamics patterns in the city of Rio de Janeiro to improve the knowledge about atmospheric behavior. The climate change already detected in different parts of the globe is mainly related to the increase in the frequency and intensity of extreme temperature and precipitation events, ratifying this type of study.

Concerning climate extremes associated with air temperature, it was found that the frequency of warm (cold) days and nights are increasing (decreasing) in the city of Rio de Janeiro. There was expressive warming from P1 to P2, then continuing by P3. Cold (Warm) extremes are changing with greater magnitude in ABOV (STCZ) than in STCZ (ABOV). Global warming and urbanization contribute to this rise in temperature. Besides, physical and social features support the manifestation of urban heat islands in the town. In terms of rainfall, there is a significant growth of total precipitation associated with heavy rainfall (+84 mm/decade) in ABOV. More floods and landslides can happen due to this trend in extreme precipitation episodes coadunate to the physiographic aspects of Rio de Janeiro. Regarding upper-level soundings trends, it is verified that there is a statistically significant elevation in air temperature at the middle troposphere and a reduction at high levels. This fact is linked to anthropic activities and their growth in the emission of greenhouse gases. There is a significant rise in the 850 hPa level for air relative humidity and a reduction in 200 and 100 hPa. There is more available evapotranspiration and moisture from the forest and ocean in the lower troposphere due to increased air temperature near the surface.

Alterations in the frequency and intensity of extreme meteorological episodes, mainly those associated with rainfall, are related to modifications in the thermodynamic panorama. There is an evident growing trend of the *K*, *TT*, and *PW* indices over the last few years in the city of Rio de Janeiro, besides a reduction in the CAPE index. The rise in the *K* index is supplied by the elevation in air temperature and humidity in the lower and medium troposphere. Moreover, the higher values of the *K* and *PW* indices are related with expressive total precipitation. The rising trends of some extreme precipitation indices in the city of Rio de Janeiro are probably related to the increasing trend of *PW* over the years. Thus, a more emphatic detection of areas susceptible to heavy precipitation events is possible with the concurrent evaluation of these indices, whether in the short-term (weather forecasting), medium-term (climatology), or long-term (climate change). The relationship between climate extremes and thermodynamic patterns can help improve nowcasting methods that have been structured through artificial intelligence. In addition, climate change trends can ratify the need for policy measures aimed at the city's resilience to extreme

events.

Therefore, this study is essential for professionals who need to deal with actions to prepare and prevent the population in the face of extreme rainfall episodes in the city of Rio de Janeiro and other places. Besides, a management plan is necessary and must include the mitigation of greenhouse gas emissions generated by large urban agglomerations, adaptation to the impacts of climate change on natural resources and urban infrastructure, and its effects on public health and economic productivity.

## Funding

The authors declare that no funds, grants, or other support were received during the preparation of this manuscript.

## Author Contributions

Wanderson Luiz-Silva wrote and structured the entire article, including the bibliographic review and the interpretation of the results. Fabricio Polifke da Silva generated the manuscript figures and analyzed the results associated with the instability indices. Claudine Pereira Dereczynski collaborated with exploring climate extremes and revised the entire paper. José Ricardo de Almeida França contributed to the conclusions and revised the article.

## Data Availability

The datasets generated during and/or analyzed during the current study are available from the organization that maintains the data on reasonable request.

## Conflicts of Interest

The authors declare that they have no known competing financial interests or personal relationships that could have appeared to influence the work reported in this paper.

## References

Allan, R., Barlow, M., Byrne, M. P., Cherchi, A. et al. (2020). Advances in Understanding Large-Scale Responses of the Water Cycle to Climate Change. *Annals of the New York Academy of Sciences, 1472,* 49-75. https://doi.org/10.1111/nyas.14337

Alvares, C. A., Stape, J. L., Sentelhas, P. C., Gonçalves, J. L. M., & Sparovek, G. (2014). Köppen's Climate Classification Map for Brazil. *Meteorologische Zeitschrift, 22,* 711-728. https://doi.org/10.1127/0941-2948/2013/0507

Barata, M. M. L., Bader, D. A., Dereczynski, C. P., Regoto, P., & Rosenzweig, C. (2020). Use of Climate Change Projections for Resilience Planning in Rio de Janeiro, Brazil. *Frontiers in Sustainable Cities, 2,* Article No. 28. https://doi.org/10.3389/frsc.2020.00028

Blanchard, D. O. (1998). Mesoscale Convective Patterns of the Southern High Plains. *Bulletin of the American Meteorological Society, 71,* 994-1005. https://doi.org/10.1175/1520-0477(1990)071<0994:MCPOTS>2.0.CO;2

Boers, N., Bookhagen, B., Marwan, N., & Kurths, J. (2015). Spatiotemporal Characteris-

tics and Synchronization of Extreme Rainfall in South America with Focus on the Andes Mountain Range. *Climate Dynamics, 46,* 601-617. https://doi.org/10.1007/s00382-015-2601-6

Bombardi, R. J., Carvalho, L. M. V., Jones, C., & Reboita, M. S. (2014). Precipitation over Eastern South America and the South Atlantic Surface Temperature during Neutral ENSO Periods. *Climate Dynamics, 42,* 1553-1568. https://doi.org/10.1007/s00382-013-1832-7

Bonnet, S. M., Dereczynski, C. P., & Nunes, A. (2018). Synoptic and Climatological Characterization of Post-Frontal Rainfall Events in Rio de Janeiro. *Revista Brasileira de Meteorologia, 33,* 547-557. https://doi.org/10.1590/0102-7786333013

Brooks, H. E., Anderson, A. R., Riemann, K., Ebbers, I., & Flachs, H. (2007). Climatological Aspects of Convective Parameters from the NCAR/NCEP Reanalysis. *Atmospheric Research, 83,* 294-305. https://doi.org/10.1016/j.atmosres.2005.08.005

Carvalho, L. M. V., Jones, C., & Liebmann, B. (2004). The South Atlantic Convergence Zone: Intensity, Form, Persistence, and Relationships with Intraseasonal to Interannual Activity and Extreme Rainfall. *Journal of Climate, 17,* 88-108. https://doi.org/10.1175/1520-0442(2004)017<0088:TSACZI>2.0.CO;2

Chung, E.-S., Soden, B., Sohn, B. J., & Shi, L. (2014). Upper-Tropospheric Moistening in Response to Anthropogenic Warming. *Proceedings of the National Academy of Sciences of the United States of America, 111,* 11636-11641. https://doi.org/10.1073/pnas.1409659111

Costa, A. J. S. T., Conceição, R. S., & Amante, F. O. (2018). The Floods and Urban Growth of Rio de Janeiro City: Studies toward an Cartography of Urban Floods. *Geo UERJ, 32,* e25685. https://doi.org/10.12957/geouerj.2018.25685

Costa, R. L., Baptista, G. M. M., Gomes, H. B., Silva, F. D. S. et al. (2020). Analysis of Climate Extremes Indices over Northeast Brazil from 1961 to 2014. *Weather and Climate Extremes, 28,* Article ID: 100254. https://doi.org/10.1016/j.wace.2020.100254

Dereczynski, C., Chou, S. C., Lyra, A., Sondermann, M. et al. (2020). Downscaling of Climate Extremes over South America—Part I: Model Evaluation in the Reference Climate. *Weather and Climate Extremes, 29,* Article ID: 100273. https://doi.org/10.1016/j.wace.2020.100273

Dereczynski, C., Luiz-Silva, W., & Marengo, J. (2013). Detection and Projections of Climate Change in Rio de Janeiro, Brazil. *American Journal of Climate Change, 2,* 25-33. https://doi.org/10.4236/ajcc.2013.21003

Derubertis, D. (2006). Recent Trends in Four Common Stability Indices Derived from US Radiosonde Observations. *Journal of Climate, 19,* 309-323. https://doi.org/10.1175/JCLI3626.1

Doswell III, C. A. (2001). *Severe Convective Storms, Meteorological Monograph*. American Meteorological Society. https://doi.org/10.1007/978-1-935704-06-5

Doswell III, C. A., & Schultz, D. M. (2006). On the Use of Indices and Parameters in Forecasting. *Electronic Journal of Severe Storms Meteorology, 1,* 1-22. https://doi.org/10.55599/ejssm.v1i3.4

Duarte, B. M., França, J. R. A., & Justo, L. A. J. (2018). The Use of CloudSat Data to Characterize the Microphysical Structure of Extreme Precipitation Events over South and Southeast of Brazil. *Anuário do Instituto de Geociências—UFRJ, 41,* 15-27. https://doi.org/10.11137/2018_1_15_27

Easterling, D. R., Meehl, G. A., Parmesan, C., Changnon, S. A. et al. (2000). Climate Extremes: Observations, Modeling and Impacts. *Science, 289,* 2068-2074.

https://doi.org/10.1126/science.289.5487.2068

Emanuel, K. A. (1994). *Atmospheric Convection*. Oxford University Press.

Frich, P., Alexander, L. V., Della-Marta, P., Gleason, B. et al. (2002). Observed Coherent Changes in Climatic Extremes during the 2nd Half of the 20th Century. *Climate Research, 19,* 193-212. https://doi.org/10.3354/cr019193

Fujita, M., & Sato, T. (2017). Observed Behaviours of Precipitable Water Vapour and Precipitation Intensity in Response to Upper Air Profiles Estimated from Surface Air Temperature. *Nature Scientific Reports, 7,* Article No. 4233. https://doi.org/10.1038/s41598-017-04443-9

Geirinhas, J. L., Russo, A., Libonati, R., Sousa, P. M. et al. (2021). Recent Increasing Frequency of Compound Summer Drought and Heatwaves in Southeast Brazil. *Environmental Research Letters, 16,* Article ID: 034036. https://doi.org/10.1088/1748-9326/abe0eb

George, J. J. (1960). *Weather Forecasting for Aeronautics*. Academic Press.

Gulev, S. K., Thorne, P. W., Ahn, J., Dentener, F. J. et al. (2021). Changing State of the Climate System. In V. Masson-Delmotte, P. Zhai, A. Pirani, S. L. Connors, C. Péan, S. Berger, N. Caud, Y. Chen, L. Goldfarb, M. I. Gomis, M. Huang, K. Leitzell, E. Lonnoy, J. B. R. Matthews, T. K. Maycock, T. Waterfield, O. Yelekçi, R. Yu, & B. Zhou (Eds.), *Climate Change 2021: The Physical Science Basis. Contribution of Working Group I to the Sixth Assessment Report of the Intergovernmental Panel on Climate Change* (pp. 287-422). Cambridge University Press.

Held, I. M., & Soden, B. J. (2006). Robust Responses of the Hydrological Cycle to Global Warming. *Journal of Climate, 19,* 5686-5699. https://doi.org/10.1175/JCLI3990.1

Helsel, D. R., & Hirsch, R. M. (1992). *Statistical Methods in Water Resources*. Elsevier.

Henry, N. L. (2000). A Static Stability Index for Low-Topped Convection. *Weather Forecast, 15,* 246-254. https://doi.org/10.1175/1520-0434(2000)015<0246:ASSIFL>2.0.CO;2

IBGE (2021). *Brazilian Institute of Geography and Statistics—Panorama Cidades e Estados*. https://www.ibge.gov.br/cidades-e-estados/rj/rio-de-janeiro.html

IPCC (2021). Technical Summary. In V. Masson-Delmotte, P. Zhai, A. Pirani, S. L. Connors, C. Péan, S. Berger, N. Caud, Y. Chen, L. Goldfarb, M. I. Gomis, M. Huang, K. Leitzell, E. Lonnoy, J.B.R. Matthews, T. K. Maycock, T. Waterfield, O. Yelekçi, R. Yu, & B. Zhou (Eds.), *Climate Change 2021: The Physical Science Basis. Contribution of Working Group I to the Sixth Assessment Report of the Intergovernmental Panel on Climate Change* (pp. 33-144). Cambridge University Press.

Kendall, M. A., & Stuart, A. (1975). *The Advanced Theory of Statistics*. Charles Griffin.

Kunkel, K. E., Karl, T. R., Squires, M. F., Yin, X. et al. (2020). Precipitation Extremes: Trends and Relationships with Average Precipitation and Precipitable Water in the Contiguous United States. *Journal of Applied Meteorology and Climatology, 59,* 125-142. https://doi.org/10.1175/JAMC-D-19-0185.1

Kunz, M. (2007). The Skill of Convective Parameters and Indices to Predict Isolated and Severe Thunderstorms. *Natural Hazards and Earth System Sciences, 7,* 327-342. https://doi.org/10.5194/nhess-7-327-2007

La Rovere, E. L., & Silva de Sousa, D. (2016). *Estratégia de adaptação às mudanças climáticas da cidade do Rio de Janeiro*. Rio Prefeitura Meio Ambiente, Rio de Janeiro.

Leyba, I. M., Solman, S. A., & Saraceno, M. (2019). Trends in Sea Surface Temperature and Air-Sea Heat Fluxes over the South Atlantic Ocean. *Climate Dynamics, 53,* 4141-4153. https://doi.org/10.1007/s00382-019-04777-2

Lopez, P. (2007). Cloud and Precipitation Parameterizations in Modeling and Variational Data Assimilation: A Review. *Journal of the Atmospheric Sciences, 64,* 3766-3784. https://doi.org/10.1175/2006JAS2030.1

Luiz-Silva, W., & Dereczynski, C. P. (2014). Climatological Characterization and Observed Trends in Climatic Extremes in the State of Rio de Janeiro. *Anuário do Instituto de Geociências—UFRJ, 37,* 123-138. https://doi.org/10.11137/2014_2_123_138

Luiz-Silva, W., & Oscar-Júnior, A. C. (2022). Climate Extremes Related with Rainfall in the State of Rio de Janeiro, Brazil: A Review of Climatological Characteristics and Recorded Trends. *Natural Hazards, 114,* 713-732. https://doi.org/10.1007/s11069-022-05409-5

Luiz-Silva, W., Oscar-Júnior, A. C., Cavalcanti, I. F. A., & Treistman, F. (2021). An Overview of Precipitation Climatology in Brazil: Space-Time Variability of Frequency and Intensity Associated with Atmospheric Systems. *Hydrological Sciences Journal, 66,* 289-308. https://doi.org/10.1080/02626667.2020.1863969

Luiz-Silva, W., Xavier, L. N. R., Maceira, M. E. P., & Rotunno, O. C. (2019). Climatological and Hydrological Patterns and Verified Trends in Precipitation and Streamflow in the Basins of Brazilian Hydroelectric Plants. *Theoretical and Applied Climatology, 137,* 353-371. https://doi.org/10.1007/s00704-018-2600-8

Mann, H. B. (1945). Non-Parametric Tests against Trend. *Econometrica, 13,* 245-259. https://doi.org/10.2307/1907187

Marengo, J. A., Souza Jr., C. M., Thonicke, K., Burton, C. et al. (2018). Changes in Climate and Land Use over the Amazon Region: Current and Future Variability and Trends. *Frontiers in Earth Science, 6,* Article No. 228. https://doi.org/10.3389/feart.2018.00228

Mears, C. A., & Wentz, F. J. (2009). Construction of the Remote Sensing Systems V3.2 Atmospheric Temperature Records from the MSU and AMSU Microwave Sounders. *Journal of Atmospheric and Oceanic Technology, 26,* 1040-1056. https://doi.org/10.1175/2008JTECHA1176.1

Miller, R. C. (1972). *Notes on Analysis and Severe Storm Forecasting Procedures of the Air Force Global Weather Center*. Technical Report 200 (Rev), Air Weather Service (MAC) United States Air Force.

Miloshevich, L. M., Vömel, H., Whiteman, D. N., & Leblanc, T. (2009). Accuracy Assessment and Correction of Vaisala RS92 Radiosonde Water Vapor Measurements. *Journal of Geophysical Research, 114,* D11305. https://doi.org/10.1029/2008JD011565

Mitovski, T., Folkins, I., von Salzen, K., & Sigmond, M. (2010). Temperature, Relative Humidity, and Divergence Response to High Rainfall Events in the Tropics: Observations and Models. *Journal of Climate, 23,* 3613-3625. https://doi.org/10.1175/2010JCLI3436.1

Nascimento, E. L. (2005). Severe Storms Forecasting Utilizing Convective Parameters and Mesoscale Models: An Operational Strategy Adoptable in Brazil? *Revista Brasileira de Meteorologia, 20,* 121-140.

Nunes, K. R. A., Abelheira, M., Gomes, O. S., Martins, P., & Aguiar, I. S. (2020). Disaster Risk Assessment: The Experience of the City of Rio de Janeiro in Developing an Impact Scale for Meteorological-Related Disasters. *Progress in Disaster Science, 5,* Article ID: 100053. https://doi.org/10.1016/j.pdisas.2019.100053

O'Gorman, P. A. (2015). Precipitation Extremes under Climate Change. *Current Climate Change Reports, 1,* 49-59. https://doi.org/10.1007/s40641-015-0009-3

O'Gorman, P. A., & Schneider, T. (2009). The Physical Basis for Increases in Precipitation

Extremes in Simulations of 21st-Century Climate Change. *Proceedings of the National Academy of Sciences of the United States of America, 106,* 14773-14777. https://doi.org/10.1073/pnas.0907610106

Pall, P., Allen, M. R., & Stone, D. A. (2007). Testing the Clausius-Clapeyron Constraint on Changes in Extreme Precipitation under $CO_2$ Warming. *Climate Dynamics, 28,* 351-363. https://doi.org/10.1007/s00382-006-0180-2

Paltridge, G., Arking, A., & Pook, M. (2009). Trends in Middle- and Upper-Level Tropospheric Humidity from NCEP Reanalysis Data. *Theoretical and Applied Climatology, 98,* 351-359. https://doi.org/10.1007/s00704-009-0117-x

Peres, L. F., Lucena, A. J., Rotunno Filho, O. C., & França, J. R. A. (2018). The Urban Heat Island in Rio de Janeiro, Brazil, in the Last 30 Years Using Remote Sensing Data. *The International Journal of Applied Earth Observation and Geoinformation, 64,* 104-116. https://doi.org/10.1016/j.jag.2017.08.012

Poujol, B., Sobolowski, S. P., Mooney, P. A., & Berthou, S. (2020). A Physically Based Precipitation Separation Algorithm for Convection-Permitting Models over Complex Topography. *Quarterly Journal of the Royal Meteorological Society, 146,* 748-761. https://doi.org/10.1002/qj.3706

Randel, W. J., Polvani, L. P., Wu, F., Kinnison, D. E. et al. (2017). Troposphere-Stratosphere Temperature Trends Derived from Satellite Data Compared with Ensemble Simulations from WACCM. *JGR Atmospheres, 122,* 9651-9667. https://doi.org/10.1002/2017JD027158

Rasmussen, E. N., & Blanchard, D. O. (1998). A Baseline Climatology of Sounding-Derived Supercell and Tornado Forecast Parameters. *Weather Forecast, 13,* 1148-1164. https://doi.org/10.1175/1520-0434(1998)013<1148:ABCOSD>2.0.CO;2

Regoto, P., Dereczynski, C., Chou, S. C., & Bazzanela, A. C. (2021). Observed Changes in Air Temperature and Precipitation Extremes over Brazil. *International Journal of Climatology, 41,* 5125-5142. https://doi.org/10.1002/joc.7119

Sapucci, L. F., Machado, L. A. T., Silveira, R. B., Fisch, G., & Monico, J. F. G. (2005). Analysis of Relative Humidity Sensor Sat the WMO Radiosonde Intercomparison Experiment in Brazil. *Journal of Atmospheric and Oceanic Technology, 22,* 664-678. https://doi.org/10.1175/JTECH1754.1

Schumacher, C., & Houze Jr., R. A. (2003). Stratiform Rain in the Tropics as Seen by the TRMM Precipitation Radar. *Journal of Climate, 16,* 1739-1756. https://doi.org/10.1175/1520-0442(2003)016<1739:SRITTA>2.0.CO;2

Schumacher, R. S., & Peters, J. M. (2017). Near-Surface Thermodynamic Sensitivities in Simulated Extreme-Rain-Producing Mesoscale Convective Systems. *Monthly Weather Review, 145,* 2177-2200. https://doi.org/10.1175/MWR-D-16-0255.1

Seidel, D. J., Free, M., & Wang, J. (2005). Diurnal Cycle of Upper-Air Temperature Estimated from Radiosondes. *Journal of Geophysical Research: Atmospheres, 110,* D9. https://doi.org/10.1029/2004JD005526

Sen, P. K. (1968). Estimates of the Regression Coefficient Based on Kendall's Tau. *Journal of the American Statistical Association, 63,* 1379-1389. https://doi.org/10.1080/01621459.1968.10480934

Shepherd, T. G. (2014). Atmospheric Circulation as a Source of Uncertainty in Climate Change Projections. *Nature Geoscience, 7,* 703-708. https://doi.org/10.1038/ngeo2253

Silva Dias, M. A. F. (1987). Sistemas de mesoescala e previsão de tempo a curto prazo. *Revista Brasileira de Meteorologia, 2,* 133-150.

Silva, F. P., Justi da Silva, M. G. A., Rotunno Filho, O. C., Pires, G. D. et al. (2019b). Synoptic Thermodynamic and Dynamic Patterns Associated with Quitandinha River Flooding Events in Petropolis, Rio de Janeiro (Brazil). *Meteorology and Atmospheric Physics, 131,* 845-862. https://doi.org/10.1007/s00703-018-0609-2

Silva, F. P., Rotunno Filho, O. C., Justi da Silva, M. G. A., Sampaio, R. J. et al. (2020). Observed and Estimated Atmospheric Thermodynamics Instability Using Radiosonde Observations over the City of Rio de Janeiro, Brazil. *Meteorology and Atmospheric Physics, 132,* 297-314. https://doi.org/10.1007/s00703-019-00688-3

Silva, F. P., Rotunno Filho, O. C., Sampaio, R. J., Dragaud, I. C. D. V. et al. (2019a). Evaluation of Atmospheric Thermodynamics and Dynamics during Heavy-Rainfall and No-Rainfall Events in the Metropolitan Area of Rio de Janeiro, Brazil. *Meteorology and Atmospheric Physics, 131,* 299-311. https://doi.org/10.1007/s00703-017-0570-5

Sneyers, R. (1990). *On the Statistical Analysis of Series of Observations*. World Meteorological Organization.

Soden, B. J., Jackson, D. L., Ramaswamy, V., Schwarzkopf, M. D., & Huang, X. (2005). The Radiative Signature of Upper Tropospheric Moistening. *Science, 310,* 841-844. https://doi.org/10.1126/science.1115602

Steiner, A. K., Ladstädter, F., Randel, W. J., Maycock, A. C. et al. (2020). Observed Temperature Changes in the Troposphere and Stratosphere from 1979 to 2018. *Journal of Climate, 33,* 8165-8194. https://doi.org/10.1175/JCLI-D-19-0998.1

Taszarek, M., Brooks, H. E., Czernecki, B., Szuster, P., & Fortuniak, K. (2018). Climatological Aspects of Convective Parameters over Europe: A Comparison of ERA-Interim and Sounding Data. *Journal of Climate, 31,* 4281-4308. https://doi.org/10.1175/JCLI-D-17-0596.1

Timmermann, A., An, S.-I., Kug, J.-S., Jin, F.-F. et al. (2018). El-Niño-Southern Oscillation Complexity. *Nature, 559,* 535-545. https://doi.org/10.1038/s41586-018-0252-6

Tremblay, A. (2005). The Stratiform and Convective Components of Surface Precipitation. *Journal of the Atmospheric Sciences, 62,* 1513-1528. https://doi.org/10.1175/JAS3411.1

Trenberth, K. E., Dai, A., Rasmussen, R. M., & Parsons, D. B. (2003). The Changing Character of Precipitation. *Bulletin of the American Meteorological Society, 84,* 1205-1217. https://doi.org/10.1175/BAMS-84-9-1205

Westra, S., Alexander, L. V., & Zwiers, F. W. (2013). Global Increasing Trends in Annual Maximum Daily Precipitation. *Journal of Climate, 26,* 3904-3918. https://doi.org/10.1175/JCLI-D-12-00502.1

Westra, S., Fowler, H. J., Evans, J. P., Alexander, L. V. et al. (2014). Future Changes to the Intensity and Frequency of Short-Duration Extreme Rainfall. *Reviews of Geophysics, 52,* 522-555. https://doi.org/10.1002/2014RG000464

Zandonadi, L., Acquaotta, F., Fratianni, S., & Zavattini, J. A. (2016). Changes in Precipitation Extremes in Brazil (Paraná River Basin). *Theoretical and Applied Climatology, 123,* 741-756. https://doi.org/10.1007/s00704-015-1391-4

Zhang, X., Feng, Y., & Chan, R. (2018). *Introduction to RClimDex v1.9*. Climate Research Division, Canada.

Zilli, M. T., Carvalho, L. M. V., & Lintner, B. R. (2019). The Poleward Shift of South Atlantic Convergence Zone in Recent Decades. *Climate Dynamics, 52,* 2545-2563. https://doi.org/10.1007/s00382-018-4277-1

Zilli, M. T., Carvalho, L. M. V., Liebmann, B., & Silva Dias, M. A. (2017). A Comprehen-

sive Analysis of Trends in Extreme Precipitation over Southeastern Coast of Brazil. *International Journal of Climatology, 37,* 2269-2279. https://doi.org/10.1002/joc.4840

Zveryaev, I. I., & Chu, P.-S. (2003). Recent Climate Changes in Precipitable Water in the Global Tropics as Revealed in National Centers for Environmental Prediction/National Center for Atmospheric Research Reanalysis. *JGR Atmospheres, 108,* D10. https://doi.org/10.1029/2002JD002476